BIOCHEMISTRY
including biophysical chemistry & molecular biology

Article

pubs.acs.org/biochemistry

Solution Structure and Dynamics of Human Hemoglobin in the Carbonmonoxy Form

Jing-Song Fan,[†] Yu Zheng,[†] Wing-Yiu Choy,[‡] Virgil Simplaceanu,[§] Nancy T. Ho,[§] Chien Ho,*[,§] and Daiwen Yang*[,†]

[†]Department of Biological Sciences, National University of Singapore, 14 Science Drive 4, Singapore 117543

[‡]Department of Biochemistry, The University of Western Ontario, London, Ontario, Canada

[§]Department of Biological Sciences, Carnegie Mellon University, Pittsburgh, Pennsylvania 15213, United States

Supporting Information

ABSTRACT: The solution structure of human adult carbonmonoxy hemoglobin (HbCO A) was refined using stereospecifically assigned methyl groups and residual dipolar couplings based on our previous nuclear magnetic resonance structure. The tertiary structures of individual chains were found to be very similar to the X-ray structures, while the quaternary structures in solution at low salt concentrations resembled the X-ray R structure more than the R2 structure. On the basis of chemical shift perturbation by inositol hexaphosphate (IHP) titration and docking, we identified five possible IHP binding sites in HbCO A. Amide−water proton exchange experiments demonstrated that αThr38 located in the $\alpha1\beta2$ interface and several loop regions in both α- and β-chains were dynamic on the subsecond time scale. Side chain methyl dynamics revealed that methyl groups in the $\alpha1\beta2$ interface were dynamic, but those in the $\alpha1\beta1$ interface were quite rigid on the nanosecond to picosecond and millisecond to microsecond time scales. All the data strongly suggest a dynamic $\alpha1\beta2$ interface that allows conformational changes among different forms (like T, R, and R2) easily in solution. Binding of IHP to HbCO A induced small structural and dynamic changes in the $\alpha1\beta2$ interface and the regions around the hemes but did not increase the conformational entropy of HbCO A. The binding also caused conformational changes on the millisecond time scale, very likely arising from the relative motion of the $\alpha1\beta1$ dimer with respect to the $\alpha2\beta2$ dimer. Heterotropic effectors like IHP may change the oxygen affinity of Hb through modulating the relative motion of the two dimers and then further altering the structure of heme binding regions.

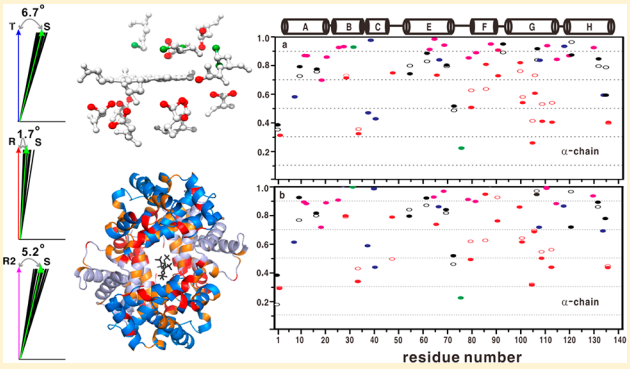

Hemoglobin (Hb) is a tetrameric protein consisting of two identical α-subunits and two identical β-subunits. It has been used as a model system in textbooks for understanding protein cooperativity, allosteric effects, and structure−function relationships. In the two-structure MWC concerted model[1] and Perutz's stereochemical model,[2] hemoglobin has been assumed to exist in two interconvertible forms, the tense (T) deoxy form and the relaxed (R) oxy form. Early X-ray crystallographic studies showed that Hbs could adopt only two stable quaternary structures, one corresponding to deoxy-Hb (T state) and the other to ligand-bound Hb (R state, e.g., in complex with oxygen or carbon monoxide). Although the R and T quaternary structures are significantly different, the tertiary structures of each subunit are nearly identical in the two forms. These studies supported the two-structure models that explained the experimental oxygen binding data. However, a number of new ligand-bound Hb structures known as R2,[3] RR2,[4] and R3[4] were later discovered by altering the crystallization conditions for human adult carbonmonoxy Hb (HbCO A). Because of the significant differences in the quaternary structure among the identified Hb structural forms, the two-structure models have been challenged. To address which quaternary structure represents the true ligand-bound state in solution, we investigated the quaternary structures of Hb in the absence and presence of the allosteric effector IHP using one-bond $^{1}H-^{15}N$ residual dipolar couplings (RDCs) assuming that the structure of each $\alpha\beta$ dimer in solution was the same as that in the crystal state. From these studies, we concluded that the solution structure of HbCO A was a dynamic intermediate between the R and R2 forms and IHP could shift the structure toward the R form.[5,6] Then, we determined a solution structure of HbCO A using an NOESY-based strategy[7] and found that the nuclear magnetic resonance (NMR) solution structures of each subunit and the $\alpha\beta$ dimer agreed well with those in the R2 or R form, but the tetramer structure was notably different from the X-ray structures.

Received: May 4, 2013
Revised: July 31, 2013
Published: July 31, 2013

On the basis of the early crystal structures of the Hb molecule,[2] it has been thought that the T form has a lower affinity for oxygen than the R form and thus the quaternary structure of Hb controls its oxygen affinity. However, recent studies demonstrated that the quaternary T and R forms did not correlate with the oxygen affinity of Hb because the T and R forms in the presence of artificial allosteric effectors L35 and inositol hexaphosphate (IHP) had nearly the same affinity for oxygen.[8,9] Because L35 could greatly reduce the oxygen affinity of Hb without switching the ligand-bound structure to the T form,[10] a dynamic allosteric model was proposed to account for the contribution of protein dynamics to oxygen affinity.[8] This model was supported by a recent molecular dynamics (MD) simulation study showing that the effector 2,3-bisphosphoglycerate (2,3-BPG) significantly increased the dynamics of Hb on a nanosecond time scale.[11] However, NMR relaxation experiments did not detect any significant IHP-induced changes in the backbone dynamics of Hb on nanosecond to picosecond time scales.[12] Instead, IHP greatly increased the backbone dynamics of HbCO A on millisecond to microsecond time scales but had nearly no effect on the dynamics of the deoxy form.[13] Here, we present the refined solution structure of HbCO A in the absence of IHP, water−amide proton exchange results, and the methyl dynamics in the absence and presence of IHP.

MATERIALS AND METHODS

Human Normal Adult Hemoglobin Samples. Chain-specifically ^{13}C- and ^{15}N-labeled HbCO A and ^{2}H- and ^{15}N-labeled HbCO A were prepared as described previously.[14] For stereospecific assignments of methyl groups of valine and leucine residues, chain-specifically and 10% fractionally ^{13}C-labeled HbCO A were prepared following the procedure described previously.[15] In the ^{1}H−^{15}N HSQC experiments with IHP titration to HbCO A, the concentration of Hb was ∼0.5 mM (in term of a tetramer) and the final IHP concentration ranged from 0 to 3 mM. In all other experiments, the concentration of Hb was ∼0.6 mM, corresponding to an effective concentration of 1.2 mM per labeled chain type (α or β). It should be mentioned that in our NMR experiments, one type of Hb chain was isotopically labeled and the other was not labeled.[14] All samples were equilibrated with a 0.1 M sodium phosphate buffer (pH 7.0) containing ∼5% D_2O and saturated with CO gas.

Stereospecific Assignment. Two-dimensional (2D) ^{1}H−^{13}C constant-time HSQC and non-constant-time HMQC spectra were collected at 30 °C on a Bruker Avance 600 MHz spectrometer using the 10% fractionally ^{13}C-labeled samples. The *pro-R* ($C^{\gamma 1}$ for Val and $C^{\delta 1}$ for Leu) and *pro-S* ($C^{\gamma 2}$ for Val and $C^{\delta 2}$ for Leu) methyl groups were assigned on the basis that *pro-R* and *pro-S* methyls give rise to doublet and singlet peaks in the HMQC spectrum, respectively. The doublet peaks in the HMQC spectrum appeared as negative singlets in the constant-time HSQC spectrum.

Water−Amide Proton Exchange. All NMR experiments for water−amide exchange and methyl dynamics were performed at 30 °C on a Bruker Avance 800 MHz spectrometer equipped with a cryogenic TXI probe. The phase-modulated CLEAN chemical exchange (CLEANEX-PM) approach with a fast HSQC (FHSQC) detection scheme[16] was employed to record ^{1}H−^{15}N HSQC spectra on the chain-specifically ^{2}H- and ^{15}N-labeled samples with a series of mixing times (5, 10, 15, and 20 ms). The effective exchange rates were calculated using the initial slope analysis.[16]

Methyl Dynamics. Methyl ^{13}C spin−lattice relaxation rates (R_1) and cross-correlated relaxation rates (Γ) were measured at 30 °C on a Bruker 800 MHz spectrometer using our recently developed methods.[17,18] In the R_1 measurements, data were acquired with four scans, a spectral width of 22 ppm in the ^{13}C (t_1) dimension, a recycle delay of 1 s, a proton saturation time of 2.5 s, and a series of relaxation delays (0.01, 0.05, 0.1, 0.2, 0.3, 0.4, and 0.6 s). In the Γ measurements, ^{1}H−^{13}C HSQC spectra were recorded with eight scans, a spectral width of 22 ppm in the t_1 dimension, a recycle delay of 2.5 s, a constant time (T) of 27.6 ms, and a series of relaxation delays (Δ) (0.012, 0.6, 1.2, 1.8, 2.4, 3.0, 3.6, 4.2, 4.8, 5.4, 6.0, 6.6, 7.2, and 8.0 ms). One duplicate spectrum at a relaxation delay of 1.2 ms was recorded to estimate the experimental errors in peak intensities for each sample; 90 t_1 increment points were used in all experiments. R_1 values were obtained by fitting the peak decay profiles to a monoexponential function. Γ values were calculated from the dependence of peak intensities on the relaxation delay (Δ) using the following equation:[17]

$$I(\Delta, T) = (3\cos(3\pi J\Delta)\exp(-4\Gamma T) + \{1 + 15\Gamma\tau_a[1 - \exp(-y\Gamma)]\}\cos(\pi J\Delta)) / (3\exp(-4\Gamma T) + \{1 + 15\Gamma\tau_a[1 - \exp(-y\Gamma)]\}) \quad (1)$$

where I is the peak intensity for a given methyl group, J is the one-bond ^{1}H−^{13}C scalar coupling constant that was determined from data fitting, τ_a is the delay used in the first INEPT period in the pulse scheme and was set to 1 ms in this study, and y is a correction factor given by the equation $y = 0.2229 - 0.0046\tau_m + 0.000052\tau_m^2$ in which τ_m is the overall tumbling time of the protein.

The measured ^{13}C relaxation rates R_1 and Γ for a specific methyl group depend on its motional properties in a protein. Using the model-free analysis, we can extract the internal motional parameters (S^2 and τ_e) from the following equations:

$$R_1 \approx 3\frac{\hbar^2\gamma_C^2\gamma_H^2}{10r_{CH}^6}\left(\frac{\mu_0}{4\pi}\right)^2[J(\omega_H - \omega_C) + 3J(\omega_C) + 6J(\omega_H + \omega_C)] + \frac{\hbar^2\gamma_C^4}{10r_{CC}^6}\left(\frac{\mu_0}{4\pi}\right)^2[J(0) + 3J(\omega_C) + 6J(2\omega_C)] + \frac{2\omega_C^2\Delta\sigma^2}{15}J(\omega_C) \quad (2)$$

$$\Gamma = \frac{\hbar^2\gamma_H^2\gamma_C^2}{10r_{CH}^6}\left(\frac{\mu_0}{4\pi}\right)^2[4J_{HCH}(0) + 3J_{HCH}(\omega_C)] + \frac{\hbar^2\gamma_H^4}{10r_{HH}^6}\left(\frac{\mu_0}{4\pi}\right)^2[3J_{HHH}(\omega_H) + 3J(2\omega_H)] \quad (3)$$

$$J_{ijk}(\omega) = \frac{S_f^2S_{axis}^2\tau_m}{1 + \omega^2\tau_m^2} + \frac{[P_2(\theta_{ij,jk}) - S_{axis}^2S_f^2]\tau_1}{1 + \omega^2\tau_1^2} \quad (4)$$

where γ_i and ω_i are the gyromagnetic ratio and Larmor frequency of spin i, respectively; $\hbar = h/2\pi$; h is Planck's constant; μ_0 is the permittivity of free space; r_{CH} is the C−H bond distance and is assumed to be 1.09 Å; r_{CC} is the C−C bond distance and is assumed to be 1.517 Å; $\Delta\sigma = \sigma_\parallel - \sigma_\perp$, where $\sigma_\parallel$ and $\sigma_\perp$ are the principal components of an axially

dx.doi.org/10.1021/bi4005683 | Biochemistry 2013, 52, 5809−5820

symmetric ^{13}C CSA tensor along the parallel and perpendicular axes, respectively, and $\Delta\sigma$ is assumed to be 25 ppm; S_{axis} is the order parameter of the methyl rotation axis; $S_f^2 = 0.111$ by assuming a tetrahedral geometry for CH_3 methyl groups; $\tau_1^{-1} = \tau_m^{-1} + \tau_e^{-1}$, in which τ_e is the effective internal correlation time and $\tau_m > 10\tau_e$; and $\theta_{ij,jk}$ is the angle between bonds ij and jk. In the case where $ij = jk$, $J_{ijk}(\omega)$ becomes the autocorrelation spectral density function and is denoted as $J(\omega)$.

Methyl ^{13}C Relaxation Dispersion. Methyl ^{13}C relaxation dispersion data were recorded on uniformly ^{13}C-labeled samples at 30 °C on a Bruker 800 MHz spectrometer using a slightly modified $^1H \rightarrow {}^{13}C \rightarrow {}^1H$ CPMG scheme.[19] To remove the effect of J coupling interactions between methyl ^{13}C and its neighboring ^{13}C spins, selective RE-BURP 180° pulses were applied during the CPMG and P-element periods. To suppress one-bond $^{13}C-{}^{13}C$ coupling during the t_1 period, a selective RE-BURP 180° pulse was inserted between the first $t_1/2$ and t_b periods. All the RE-BURP pulses had a duration of 1 ms. The RE-BURP pulse used during the t_1 period was centered at 40 ppm, while others were centered at 15 ppm. Using this modified scheme, we could obtain only Ala, Met, and Thr methyl relaxation dispersion profiles because the J coupling effect could not be effectively suppressed for other methyl groups in uniformly ^{13}C-labeled samples. The dispersion profiles were obtained from 10 spectra recorded with 24 scans, a recycle delay of 1.5 s, 90 increments, and a spectral width of 22 ppm in the t_1 dimension, a constant relaxation delay T of 33 ms, and a series of ν_{CPMG} fields (60.6, 121.2, 181.8, 242.4, 303.0, 363.6, 424.2, 484.8, 545.4, and 606.0 Hz). A reference spectrum was recorded to calculate the effective relaxation rate (R_2^{eff}) of a methyl ^{13}C when T was set to zero. One duplicate spectrum at a ν_{CPMG} value of 181.8 Hz was also recorded to estimate the errors in R_2^{eff}.

All data were processed with nmrPipe[20] and analyzed with Sparky (T. D. Goddard and D. G. Kneller, *SPARKY 3*, University of California, San Francisco, CA).

Structure Recalculation. Using distance constraints derived from NOEs, dihedral angle restraints, hydrogen bond constraints derived from water−amide exchange, and residual dipolar coupling (RDC) constraints from a stretched polyacrylamide gel, we recalculated the HbCO A structures with the xplor-nih[21] using two methods. In the first method (or conventional method), backbone torsion angles (Φ and Ψ) derived from the chemical shifts were employed as the dihedral angle restraints, and the tolerance for each torsion angle is ±20°. In the second method (or nonconventional method), Φ and Ψ from the X-ray structure [Protein Data Bank (PDB) entry 1BBB, 1.7 Å resolution] were used as the restraints, and the tolerance was set to ±3°. For both methods, the RDCs that are located in helices were randomly divided into two data sets. Approximately 80% of the selected $^{15}N-{}^1H$ RDCs (work part) were included in the calculation. The remaining 20% of the RDCs (free part) were used for structure validation. For comparison, the structures were also calculated in the absence of RDC constraints with the two methods. PALES[22] was used to analyze the final 20 lowest-energy structures. The calculation protocols are available from the authors upon request.

Molecular Docking. AutoDock Vina[23] with the AutoDockTools 1.5.4[24] graphical interface was used to determine the potential binding sites of HbCO A for IHP. One solution structure of HbCO A derived from this study was chosen as the receptor, and the standard charging method within AutoDockTools was employed. The coordinates of IHP extracted from PDB entry 2K8R were used directly. The grid box (30 Å × 30 Å × 30 Å) was employed to search the possible binding sites around the whole surface (mainly focused on the six interfaces, i.e., $\alpha1\alpha2$, $\beta1\beta2$, $\alpha1\beta1$, $\alpha1\beta2$, $\alpha2\beta1$, and $\alpha2\beta2$, which showed significant chemical shift perturbation upon IHP binding) and the central region of HbCO A. Default parameters were utilized to find the best binding models. PyMOL (http://www.pymol.org) was used to analyze the data and plot the figures.

RESULTS AND DISCUSSION

Stereospecific Assignment. Using 2D $^1H-{}^{13}C$ nonconstant-time HMQC and constant-time HSQC spectra recorded on the 10% fractionally ^{13}C-labeled samples, we determined the stereospecific assignments of all Val and Leu methyls (except for βLeu106) in the α- and β-chains of HbCO A (Figure S1 of the Supporting Information).

Quaternary Structure. Previously, we determined a solution structure of HbCO A with dihedral angle restraints derived only from chemical shifts and NOE restraints[7] without stereospecific assignments. With the availability of stereospecific assignments of methyl groups, N−H residual dipolar coupling constants that were measured in a stretched polyacrylamide gel,[6] and hydrogen bond constraints, we recalculated the structure of HbCO A. The tertiary structures obtained by the conventional method in the presence or absence of RDC constraints are very similar to the X-ray structures (data not shown), but the RDC Q factors for the 20 lowest-energy structures that were refined with RDCs are abnormal (Table S1 of the Supporting Information). The 80% RDCs used in our structure calculation displayed nearly perfect consistency between the experimental and calculated RDCs, but the remaining 20% RDCs not used in the calculation showed a great discrepancy (Table S1 of the Supporting Information). Moreover, the Q factors of the unused 20% RDCs for the refined structures were even larger than the overall Q factors for the unrefined structures. Therefore, we concluded that this method gives priority to local structural adjustments rather than to the adjustment of the relative subunit−subunit orientations during the structure calculation. To overcome this problem, we implemented a nonconventional method, i.e., using very tight dihedral angle restraints with a small tolerance (±3°) and a high weighting factor. Because the tertiary structures of individual chains determined with the conventional method are very similar to the X-ray structures, Φ and Ψ angles derived from the X-ray structure (PDB entry 1BBB) were employed as the input dihedral angles in this nonconventional protocol. The results show great improvement in terms of Q factors (Table S1 of the Supporting Information). The final constraints used and structural statistics obtained are listed in Table 1.

The overall quaternary structure of HbCO A in solution obtained here (Figure S2 of the Supporting Information) is more similar to the X-ray R structure of HbCO A than to the R2 structure. The C_2 symmetry axes of the 20 lowest-energy NMR structures are close to the C_2 axis of the R structure (Figure 1a−d). The angles between the C_2 axes of the R and R2, R and T, and T and R2 structures are 5.5°, 7°, and 11.2°, respectively. The angles between the C_2 axes of the R structure and the 20 solution structures are in the range of 0.4−4.0° (Figure 1b), and the average angle is 1.7°. The average angles between the C_2 axes of the R2 and 20 solution structures and the T structure and the 20 solution structures are 5.2° and 6.7°, respectively (panels c and d of Figure 1, respectively). For the switch region of the $\alpha1\beta2$ interface, the NMR structures are

dx.doi.org/10.1021/bi4005683 | *Biochemistry* 2013, 52, 5809−5820

Table 1. Structural Statistics for the Final 20 Conformers of HbCO A[a]

distance restraints	
intraresidue ($i - j = 0$)	2740
sequential ($\|i - j\| = 1$)	1732
medium-range ($2 \leq \|i - j\| \leq 4$)	1356
long-range ($\|i - j\| \geq 5$)	1114
heme−subunit	218
intersubunit	152
hydrogen bond	472
total	7754
dihedral angle restraints	
ϕ	520
ψ	520
residual dipolar coupling restraints N−H (work/free)	298 (242/56)
dipolar coupling Q factor (%)[b]	
work (used)	6.9
free (unused)	25.3
average rmsd from the mean structure (Å)[c]	
global (tetramer)	2.36 ± 1.31 (2.65 ± 1.19)[d]
α-chain	0.69 ± 0.19 (1.34 ± 0.18)
β-chain	0.64 ± 0.18 (1.26 ± 0.19)
$\alpha\beta$ dimer	0.93 ± 0.34 (1.46 ± 0.31)
ϕ/ψ space[e]	
most favored region (%)	83.5
additionally allowed region (%)	12.9
generously allowed region (%)	3.0
disallowed region (%)	0.6
rmsd from covalent geometry	
bonds (Å)	0.0028 ± 0.00004
angles (deg)	0.4233 ± 0.0078
impropers (deg)	0.4712 ± 0.0114
rmsd from experimental restraints	
NOEs (Å)	0.03 ± 0.016
dihedral angles (deg)	0.58 ± 0.018

[a]Selected from 100 calculated conformers according to overall energy. The restraints are for the four chains (i.e., a tetramer). [b]Q factor calculated with the same method as that used in Table S1. [c]Calculated with MOLMOL.[46] Residues in all α-helical regions were used (i.e., helices A−C and E−H for the α-chain and helices A−H for the β-chain). [d]Averages are over heavy backbone atoms (all heavy atoms). [e]Calculated with PROCHECK-NMR.[47]

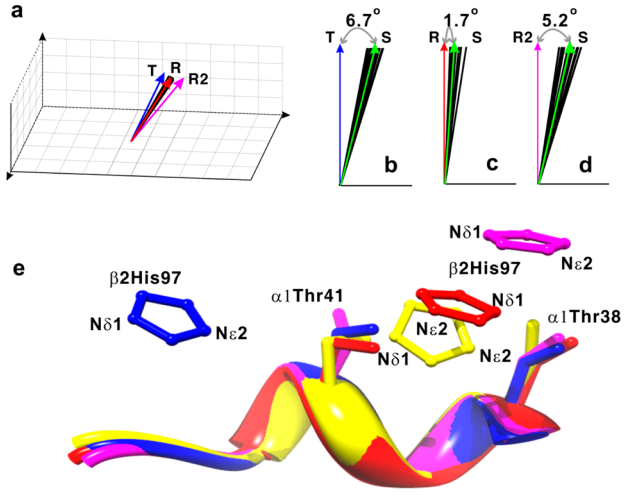

Figure 1. Comparison of the symmetric axis orientations (a−d) and the switch region in the $\alpha1\beta2$ interface (e) of HbCO A in the T, R, R2, and solution conformations. (a) Distribution of the C_2 axes of different structures in a three-dimensional frame. The angles shown in panels b−d are not drawn to scale and are enlarged for better visualization. The C_2 axes of the T, R, R2, and 20 solution conformations are shown as blue, red, magenta, and black lines. Angles between the C_2 axes of the T structure and the 20 lowest-energy NMR structures (b), between the C_2 axes of the R structure and the 20 lowest-energy NMR structures (c), and between the C_2 axes of the R2 structure and the 20 lowest-energy NMR structures (d). The average direction of the C_2 axes of the solution structures is denoted by a green arrow in panels b−d. The switch regions in the T, R, R2, and one representative solution conformation are colored blue, red, magenta, and yellow, respectively, in panel e. The backbone atoms of residues 38−44 in the $\alpha1$ subunit are superimposed to illustrate the relative orientation of $\beta2$His97.

quite similar to the R and R2 structures and very different from the T structure in terms of the location of $\beta2$His97 (Figure 1e). These results indicate that the solution structure is closer to the R structure.

Safo et al.[4] reported that the R2 structure could also be crystallized under high-salt conditions (similar to conditions used to obtain the classical R structure[2]). Mueser et al.[25] reported that the R structure of bovine HbCO was not unique but depended on the crystallization conditions. By a comparison of the geometric coordinates of the T, R, and R2 structures, Srinivasan and Rose[26] concluded that in going from the deoxy to the ligated form, the quaternary structures went from T to R, and then to R2; i.e., R was the intermediate state during the ligation process. It has been pointed out that different R-type structures could coexist in equilibrium under either high-salt or low-salt conditions and different crystal forms may simply reflect subtle differences in crystallization conditions.[4,25] These NMR structures illustrate that HbCO A can exist in multiple conformations in solution and they are more similar to the R quaternary structure. Although one can argue that the structural variations in solution result from insufficient constraints, we will show later in this paper that the interface is quite dynamic over a wide range of time scales and the dynamics can result in the multiple quaternary structures of HbCO A in solution.

Effect of IHP on the Structure of HbCO A. Titration of IHP to the chain-specifically ^{2}H- and ^{15}N-labeled and ^{13}C- and ^{15}N-labeled HbCO A showed that while several ^{1}H−^{15}N and ^{1}H−^{13}C cross-peaks displayed progressive chemical shift changes (Figure S3a,b of the Supporting Information), most ^{1}H−^{15}N cross-peaks were only slightly affected and most ^{1}H−^{13}C cross-peaks did not shift at all. From the dependence of chemical shift perturbations on IHP concentration (Figure S3c of the Supporting Information), the binding affinity should be submillimolar, although it could not be quantified because the number of IHP binding sites is unknown. A previous ^{31}P NMR study found the affinity of IHP for HbCO was ~50 μM,[28] consistent with our titration data. The chemical shift perturbations for different amino acid residues are shown in Figure 2. The residues with significant chemical shift changes (larger than the average value) in backbone NH and/or side chain CH_3 are mainly located in four regions. The first region is around the N-terminus (e.g., αVal1, αSer3, αLys7, αAsn9, βVal1, and βLeu3) and the C-terminus (αThr137, βHis143, and βHis146). The second region is around the EF loop (e.g., αAsn78, αAla79, βLys82, and βGly83). The third region is in the $\alpha1\beta2$ interface around the switch region or αC helix−βFG corner (e.g., αThr38, αThr39, αThr41, βLeu96, βAsp99, and

dx.doi.org/10.1021/bi4005683 | Biochemistry 2013, 52, 5809−5820

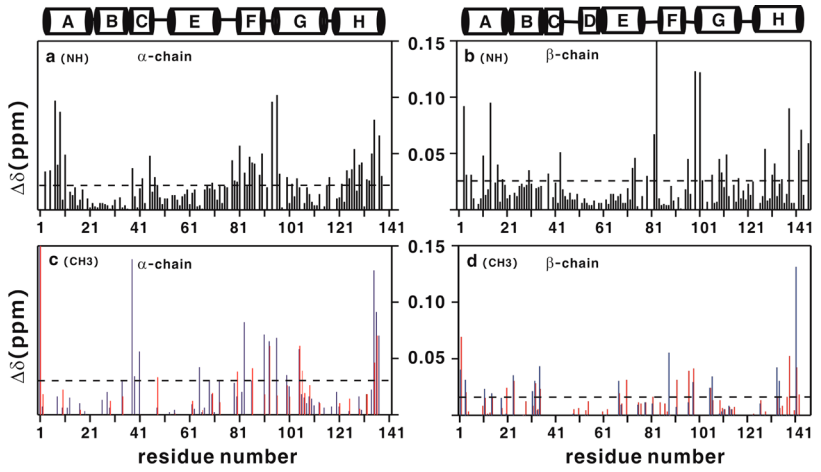

Figure 2. Chemical shift perturbations of backbone amides and side chain methyl groups by the binding of IHP to HbCO A. The chemical shift perturbations were defined as $\Delta\delta_{av} = [(\Delta\delta_{HN}^2 + \Delta\delta_N^2/25)/2]^{0.5}$ for amide NH[27] and $\Delta\delta_{av} = [(\Delta\delta_{HC}^2 + \Delta\delta_C^2/4)/2]^{0.5}$ for methyl groups, where δ_{HN}, δ_N, δ_{HC}, and δ_C are the chemical shift differences of amide ^{1}H, amide ^{15}N, methyl ^{1}H, and methyl ^{13}C, respectively, between the samples in the presence of 3 mM IHP and in the absence of IHP. The empty regions indicate that no information is available for residues in those regions because the NH and CH HSQC peaks of those residues were invisible or unassigned. The residues containing no methyl groups are located in the empty regions, too. For Leu and Val, the data for γ_1 and δ_1 methyl groups are shown with blue bars while the data for γ_2 and δ_2 methyl groups with red bars. Other methyl groups are displayed with red bars. The dashed lines represent the mean values over all residues with perturbation data.

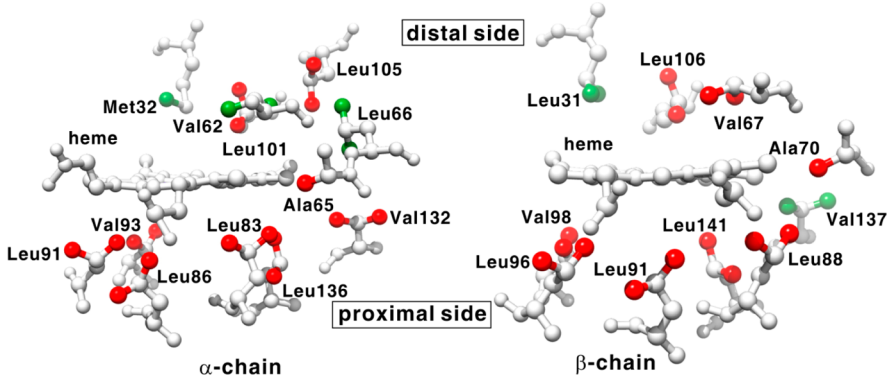

Figure 3. Heme and its proximal methyl-containing residues in the α-chain and β-chain. Methyl carbon atoms displaying significant and insignificant chemical shift perturbations are colored red and green, respectively.

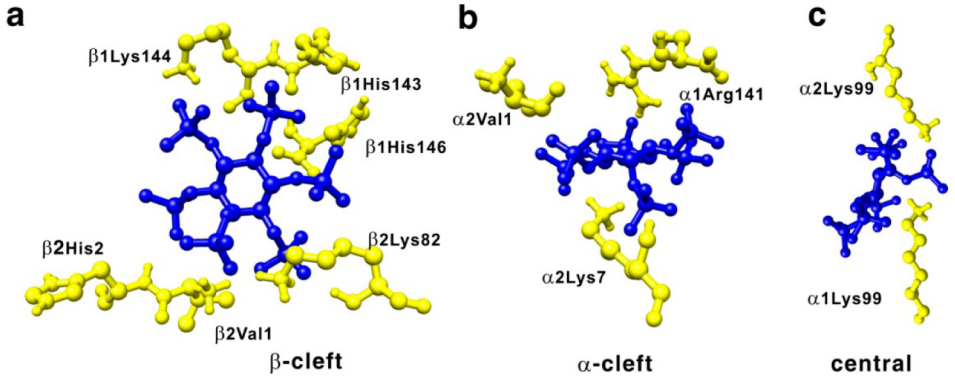

Figure 4. IHP binding sites in the β-cleft (a), α-cleft (b), and center cavity (c). The IHP molecule is shown as a blue stick.

βGlu101) and around the joint region or αFG corner−βC helix (e.g., αAsp94, αVal96, αAsn97, αLeu100, and βPhe41). The fourth region is around the heme group (e.g., αAla65, αLeu83, αLeu86, αLeu93, αLeu136, βVal67, βAla70, βLeu88, βLeu98, and βLeu141) (Figure 3).

According to the chemical shift perturbations, many of the perturbed residues are not located on the protein surface (Figure S2 of the Supporting Information). This indicates that IHP binding causes slight structural changes for the regions far from the binding sites, and determination of the binding sites from the perturbation data alone is very difficult. Thus, we performed docking of IHP to the protein with AUTODOCK[23,24] based on the NMR structure determined here. We found two potential binding sites in the β-cleft that are

dx.doi.org/10.1021/bi4005683 | *Biochemistry* 2013, 52, 5809−5820

located at the entrance of the central cavity, two in the α-cleft, and one inside the central cavity (Figure 4 and Figure S2 of the Supporting Information). Each site in the β-cleft involves six positively charged groups: β1Val1, β1His2, β1Lys82, β2Lys144, β2His143, and β2His146 in one site and β1His143 and β1His146, β2Val1, β2His2, β2Lys82, and β1Lys144 in the other (Figure 4a and Figure S2b of the Supporting Information). Each site in the α-cleft involves only three positively charged groups: α1Val1, α1Lys7, and α2Arg141 in one site and α1Arg141, α2Val1, and α2Lys7 in the other (Figure 4b and Figure S2a of the Supporting Information). Note that the N-terminal amino group of a polypeptide is positively charged. Overall, the docking results are consistent with the chemical shift perturbation result (Figures 2 and 4). The methyl groups of αVal1 and βVal1 and the backbone amide groups of αLys7, βLys82, βHis143, and βHis146 displayed very large chemical shift changes upon IHP binding (note that the amides/amine from αArg141, βVal1, and βHis2 were not detectable in the $^{15}N-^{1}H$ HSQC spectrum in the absence of IHP on an 800 MHz NMR spectrometer). Because the protein was assumed to be rigid in the docking process, the positively charged N-terminal amino group of the α-chain did not interact with the negatively charged IHP directly (Figure 4b). It is likely that a direct charge−charge interaction may exist by reorientation of the N-terminus of the α-chain that is very flexible in the absence of IHP. The chemical shift of the backbone amide of βLys144 did not change significantly, implying that only the side chain of βLys144 is involved in the interaction with IHP while its backbone is some distance from IHP. Besides βLys144, other binding residues located in the β-cleft were also found previously to be involved in the binding of IHP to the deoxy T state Hb.[29]

A recent computational study proposed that IHP binds to the α1 and α2 chains via interactions with α1Lys99, α1Arg141, α2Lys99, and α2Arg141 in the ligated R state Hb.[30] Our docking also identified this binding site, i.e., the binding site inside the central cavity, but αArg141 did not participate in the interaction with IHP in our model (Figure 4c and Figure S2c of the Supporting Information). In most X-ray structures, α1Lys99 (located inside the central cavity of the Hb tetramer) is more than 15 Å from α1Arg141 that is exposed to solvent; it seems that IHP (the largest separation between two oxygen atoms in IHP is ∼10 Å) cannot be held tightly by these four charged residues without conformational changes in the protein. When the dihedral angles around αArg141 are allowed to change by a few degrees, the charged αArg141 and αLys99 side chains can interact simultaneously with IHP. In solution, the C-terminal region (αLys139−αArg141) of the α-chain could not be observed on an 800 MHz NMR spectrometer, but αArg141 gave rise to weak signals on a 500 MHz NMR spectrometer in the absence of IHP, indicating that this region is flexible on millisecond to microsecond time scales. In the presence of IHP, the $^{1}H-^{15}N$ correlation of αLys99 disappeared, indicating that αLys99 was influenced by IHP via direct interaction or an allosteric effect. In addition, the residues proximal to αLys99 and αArg141 displayed significant chemical shift changes upon IHP binding. Thus, it is possible that α1Arg141 and α2Arg141 move in toward the cavity in solution and then interact with one IHP molecule together with α1Lys99 and α2Lys99.

Nearly all of the methyl groups around the heme in HbCO A displayed significant chemical shift changes upon IHP binding. Binding of IHP to any of the binding sites discussed above would not involve direct interaction of IHP with the heme or the methyl groups situated in the vicinity of the heme. Thus, the chemical shift perturbation for these methyl groups should result from slight tertiary structural changes around the heme induced by the heterotropic effector IHP. This is consistent with the previously proposed model, i.e., heterotropic effectors alter the tertiary structure of Hb and in turn change the function or oxygen binding affinity.[9,31] Besides the chemical shift perturbation around the hemes, many residues located in the α1β2 interface and several residues in the α1β1 interface displayed significant chemical shift changes upon IHP binding. These shift changes should not be caused by the direct interaction with IHP either but induced by alteration of the quaternary structure. This agrees very well with our results obtained from the recent RDC and backbone relaxation studies.[6,12] Therefore, the binding of IHP to Hb alters not only the tertiary structures around the heme groups but also the quaternary structure. It seems that the heterotropic effectors regulate the affinity of Hb for its ligands (like O_2 and CO) through modulation of both the tertiary and quaternary structures.

Amide−Water Exchange. Table 2 lists the amide−water proton exchange results obtained from exchange profiles (Figure S4 of the Supporting Information) using the CLEANEX-PM experiment for all measurable residues in HbCO A. Residues with amide−water proton exchange rates slower than 1 s^{-1} could not be detected by this method. Only ∼10% of the amides showed relatively large amide−water

Table 2. Water−Amide Proton Exchange Rates for HbCO A in the Absence and Presence of IHP

residue	k_{ex} (s^{-1}) without IHP	k_{ex} (s^{-1}) with IHP	intrinsic k_{ex} (s^{-1})[b]
αAla5	15.7 ± 0.1	34.2 ± 1.0	15.0
αHis20	2.6 ± 0.2	2.5 ± 0.1	43.7
αGly22	34.7 ± 0.2	35.3 ± 0.6	48.6
αThr38	38.3 ± 0.7	19.3 ± 0.8	12.8
αHis45	5.4 ± 0.1	4.6 ± 0.4	25.1
αHis50	60.3 ± 0.3	52.0 ± 0.8	87.2
αGly51	43.7 ± 0.4	39.9 ± 0.6	119.0
αSer52	2.3 ± 0.1	2.4 ± 0.1	90.5
αAla53	63.1 ± 0.9	66.1 ± 0.5	52.1
αGln54	6.1 ± 0.1	6.8 ± 0.2	30.0
αAsp74	3.7 ± 0.1	3.7 ± 0.1	9.5
αAla82	35.6 ± 0.1	19.5 ± 0.2	52.1
αAla115	11.1 ± 0.2	11.5 ± 0.3	15.0
βLeu3	4.3 ± 0.3	1.5 ± 0.1	16.8
βGlu6	3.7 ± 0.1	5.5 ± 0.4	4.7
βAsn19	4.8 ± 0.2	5.6 ± 0.1	58.4
βPhe41	−[a]	40.4 ± 2.0	24.9
βSer44	28.8 ± 0.5	48.7 ± 0.7	43.5
βAsp47	4.2 ± 0.1	7.5 ± 0.2	17.3
βAsp52	1.3 ± 0.1	4.0 ± 0.2	7.6
βLeu78	−[a]	1.2 ± 0.1	16.8
βAsp79	6.4 ± 0.2	5.7 ± 0.1	10.2
βLeu81	59.6 ± 0.8	19.4 ± 0.8	14.3
βLys82	14.8 ± 0.3	−[a]	14.7
βThr87	16.9 ± 0.4	17.1 ± 0.3	22.2
βLys120	5.2 ± 0.2	7.2 ± 0.4	35.2

[a]Exchange rates of <1 s^{-1}, which are undetectable. [b]Intrinsic exchange rates derived using SPHERE (http://www.fccc.edu/research/labs/roder/sphere/).

dx.doi.org/10.1021/bi4005683 | *Biochemistry* 2013, 52, 5809−5820

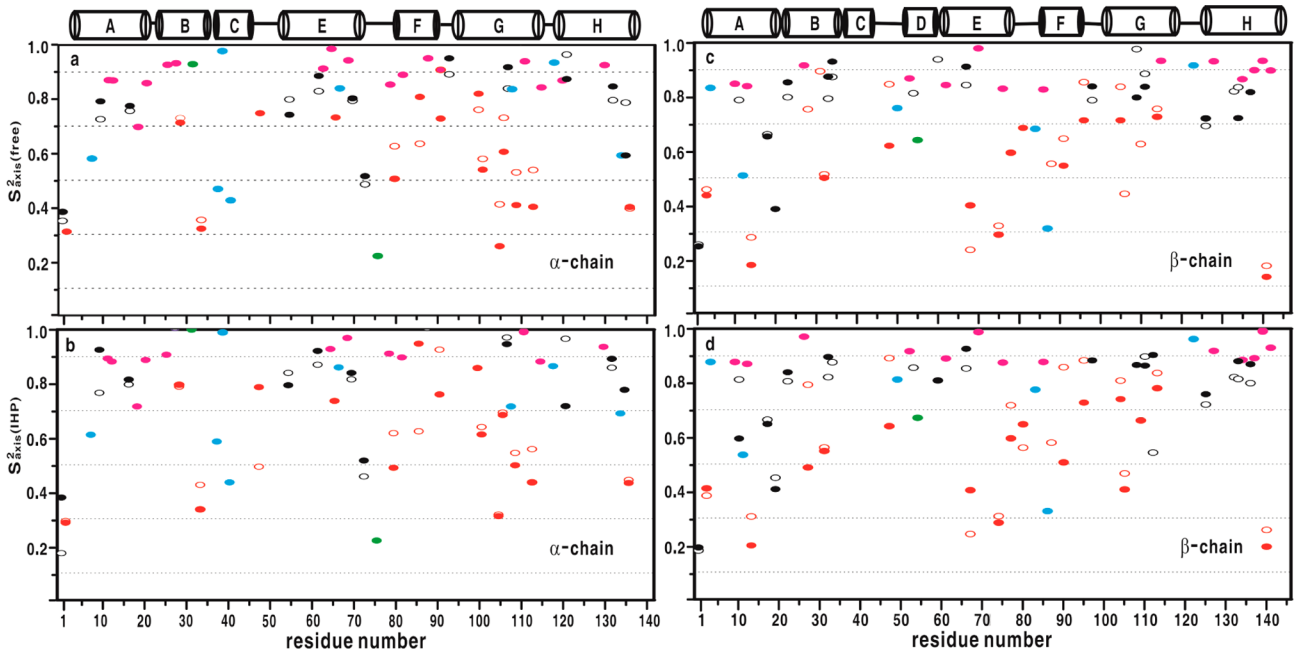

Figure 5. Order parameters (S_{axis}^2) describing the degree of spatial restriction of the C_3 symmetric axis for methyl groups in the α-chain (a) and β-chain (c) in the absence of IHP and in the α-chain (b) and β-chain (d) in the presence of IHP. The uncertainties in S_{axis}^2 for most methyl groups were ~0.01, and the maximal uncertainty was ~0.02. The empty and filled circles represent *pro-R* and *pro-S* methyl groups for Val and Leu, respectively. Data for Ala, Leu, Met, Thr, and Val methyls are colored magenta, red, green, light blue, and black, respectively.

proton exchange rates under our experimental condition (pH 7.0 and 30 °C). These amides are distributed mainly in the N-terminal regions, AB connection (αAla19−αHis20 and βVal18−βAsn19), αCD−βCE loop (αPro44−αSer52 and βPhe41−βAsp52), EF loop (αHis72−αSer81 and βLeu78−βThr87), and GH loop (αPro114−αPhe117 and βPhe118−βPhe122). The exchange results show that the loops and N-termini of the α- and β-chains are dynamic on second to millisecond time scales. According to the R and R2 structures of HbCO A, all amides with measurable exchange rates in the absence of IHP, with the exception of αHis20 and αSer52, do not form hydrogen bonds, demonstrating that the tertiary structure of HbCO A in solution is very similar to the crystal R and R2 structures. The amides of αHis20 and αSer52 had detectable exchange rates, indicating that they may not be involved in hydrogen bonding in solution, although they can form hydrogen bonds with the respective backbone oxygen atoms located at αVal17 and αSer49 in the crystal structures. The difference for these two residues between the solution and crystal structures is further supported by a previous backbone dynamics study,[12] which suggested that the backbone amides of αHis20 and αSer52 are significantly more mobile than the amides in regular helices on picosecond to nanosecond time scales. Interestingly, αThr38 located in the $\alpha1\beta2$ interface displayed a very large exchange rate, indicating that the interface around this residue is accessible to water and dynamic on the second to millisecond time scale.

When IHP binds, the exchange rates for most amides remained nearly unchanged, showing that the interaction of HbCO A with IHP does not alter the secondary structure significantly. However, several residues displayed significant changes in the exchange rates. αAla5, βPhe41, and βSer44 showed increases larger than 10 s^{-1}, while αThr38, αAla82, βLeu81, and βLys82 displayed decreases of more than 10 s^{-1} (Table 2). Because βLeu81 and βLys82 are located in one possible IHP binding site, IHP binding may reduce the access of water to the amides of βLeu81 and βLys82 and in turn causes a significant reduction of the amide−water exchange rates for these two residues. Because αAla5 is near a possible IHP binding site in the α-cleft, the change in its NH−water exchange rate may result from IHP-induced structural changes around the binding site. According to the chemical shift perturbations (Figure 2), the binding of IHP perturbs the structure of the αF helix. The slight structural alteration in this helix may contribute to the change in the exchange rate for αAla82 (located at the beginning of the αF helix). αThr38 is located in the $\alpha1\beta2$ switch region, while βPhe41 and βSer44 are in the joint region. Significant changes in the exchange rates for these residues further indicate that the $\alpha1\beta2$ interface structure (quaternary structure) is altered upon IHP binding.

Order Parameters of Methyl Groups. Methyl ^{13}C R_1 and Γ values were determined for HbCO A in the absence and presence of IHP. Only cross-peaks in the $^1H-^{13}C$ HSQC spectrum without overlap were analyzed. Methyl groups involved in strong J coupling interactions with their respective adjacent ^{13}C spins were excluded in our analysis. Because the rotational motion of HbCO A in solution is nearly isotropic,[12] an isotropic overall motional model (with an overall correlation time of 31 ns determined from ^{15}N relaxation data using the previous method[32]) was used in the extraction of order parameters from the R_1 and Γ values. Values of S_{axis}^2 were calculated for 81 of 94 methyl groups in the α-chain and 79 of 95 methyl groups in the β-chain of HbCO A in the absence of IHP, and for 76 methyl groups in the α-chain and 83 methyl groups in the β-chain of HbCO A in the presence of IHP. The order parameter data are shown in Figure 5 for the α- and β-chains. The S_{axis}^2 values are distributed in wide ranges, from ~0.2 to ~1 for the α-chain (Figure 5a,b) and from ~0.1 to ~1 for the β-chain (Figure 5c,d). For a given methyl-containing residue, the S_{axis}^2 value of the methyl group depends not only

dx.doi.org/10.1021/bi4005683 | *Biochemistry* 2013, 52, 5809−5820

Table 3. Average S_{axis}^2 Values for Ala, Thr, Val, and Leu Residues and S_{axis}^2 Values for Met Residues in the Absence and Presence of IHP

	Ala	Thr	Val	Leu	Met
α-chain without IHP	0.87 ± 0.07	0.70 ± 0.20	0.71 ± 0.17	0.55 ± 0.18	M32, 0.90 M76, 0.21
α-chain with IHP	0.87 ± 0.07	0.68 ± 0.17	0.72 ± 0.20	0.57 ± 0.19	M32, 0.94 M76, 0.21
β-chain without IHP	0.86 ± 0.05	0.65 ± 0.22	0.73 ± 0.18	0.52 ± 0.22	M55, 0.62
β-chain with IHP	0.87 ± 0.06	0.67 ± 0.22	0.73 ± 0.19	0.54 ± 0.22	M55, 0.63

on the backbone mobility of this residue but also on how far the methyl group is from the backbone.[33] To correct for the positional dependence, averages of the S_{axis}^2 values for each methyl type ($\langle S_{axis}^2 \rangle$) were used to analyze the difference between S_{axis}^2 and its corresponding $\langle S_{axis}^2 \rangle$. The $\langle S_{axis}^2 \rangle$ values in the absence and presence of IHP are listed in Table 3. As there are only two Met residues in the α-chain and there is only one Met residue in the β-chain, their S_{axis}^2 values instead of $\langle S_{axis}^2 \rangle$ are listed in Table 3.

Methyl Dynamics on Picosecond to Nanosecond Time Scales in the Absence of IHP. The S_{axis}^2 values of Ala methyl groups reflect the mobility of Ala $C_\alpha - C_\beta$ bonds, i.e., representing the backbone dynamics of Ala residues. Similar to backbone S^2 values measured from ^{15}N relaxation, the S_{axis}^2 values are distributed in a small range. Only αAla19 in the A−B connection had a significantly smaller S_{axis}^2 value (0.67). ^{15}N relaxation data also indicate that a couple of residues in this short loop are more flexible than other loop regions.[12]

Unlike backbone order parameters, S_{axis}^2 values for Thr, Val, and Leu methyl groups did not correlate with the secondary structure. Many residues located in the α-helical elements had small S_{axis}^2 values, while some residues located in the loop regions showed relatively large S_{axis}^2 values. Nevertheless, methyl order parameters for Thr, Val, and Leu residues correlated well with the tertiary and quaternary structures as discussed below.

The methyl groups of αThr39 and αThr108 are completely buried inside the protein molecule according to the R, R2, and NMR structures; their S_{axis}^2 values were 0.95 and 0.81, respectively, and were significantly larger than the average (0.70). On the other hand, the S_{axis}^2 values for some partially solvent-exposed Thr methyl groups (e.g., 0.58 for αThr8, 0.51 for βThr12, and 0.31 for βThr87) were smaller than the average. Although αThr67, αThr118, βThr4, βThr50, and βThr123 are partially solvent-exposed, their S_{axis}^2 values were 0.81, 0.91, 0.81, 0.73, and 0.89, respectively, significantly larger than the averages (0.70 for the α-chain and 0.65 for the β-chain) (Figure S5a,c of the Supporting Information). Interestingly, in both the R and R2 structures, the side chain oxygen atoms of αThr118, βThr4, βThr50, and βThr123 can form hydrogen bonds with their proximal backbone NH hydrogen atoms of αVal121, βGlu7, βAla53, and βVal126, respectively (hydrogen bonds are defined with the criteria $r_{H(N)O} < 2.4$ Å and $\theta_{HNO} < 35°$). The side chain of αThr67 can form a hydrogen bond with the side chain NεHε hydrogen of αTrp14 only in the R2 structure, not in the R structure. If the side chain of a Thr residue is involved in hydrogen bonding, the motion of the $C_\beta - C_\gamma$ bond is greatly restricted and the S_{axis}^2 value should be quite large, similar to what we observed for CH_2 groups in some Asp, Gln, and Ser residues, of which side chains form H-bonds in drkN SH3 domain.[33] Although the accuracy of the NMR structure is not good enough for determining the presence of a hydrogen bond between two atoms, the dynamics data obtained here indicate that the side chains of αThr67, αThr118, βThr4, βThr50, and βThr123 are involved in hydrogen bonding in solution. αThr38 and αThr41 are located in the α1β2 interface, and their S_{axis}^2 values were 0.47 and 0.43, respectively, significantly smaller than the average (0.70). The side chain oxygen atom of αThr41 is predicted to form a hydrogen bond with the side chain NH_2 hydrogen atom of βArg40 only in the R structure, not in the R2 structure. The dynamics result clearly indicates that there is no hydrogen bonding between αThr41 and βArg40 and the α1β2 interface is quite flexible on the nanosecond to picosecond time scale in solution. The high S_{axis}^2 value of αThr67 and the low value of αThr41 indicate that the local structure at these two residues in solution resembles more closely the R2 structure than the R structure, although the overall solution structure is more similar to the R than the R2 structure in terms of the relative orientation of the two αβ dimers.

Most of the methyl groups of Leu and Val also have S_{axis}^2 values larger than the averages when they are buried inside, while they have S_{axis}^2 values smaller than the averages when they are solvent-exposed. However, several methyl groups do not follow this trend. The methyl groups of αLeu2, αLeu105, αLeu109, βLeu3, βLeu14, βLeu68, and βLeu75 are nearly completely buried, yet their S_{axis}^2 values were significantly smaller than the averages. A similar phenomenon was observed previously for one Leu residue in the PLCC SH2−peptide complex.[34] αLeu2 and βLeu3 are located at the N-termini, and their backbone amides were shown to be quite flexible.[12] Thus, the low S_{axis}^2 values for these two residues should be caused by the high backbone mobility. αLeu105, αLeu109, βLeu14, βLeu68, and βLeu75 are located in regular helices with high backbone rigidity. The high mobility of these buried Leu methyl groups can result from local breathing motion or/and the presence of internal cavities around these residues.[34] On the other hand, αLeu91 and βLeu96 methyl groups are partially exposed to solvent, but the S_{axis}^2 values were 0.88, 0.71, 0.83, and 0.69 for αLeu91δ1, αLeu91δ2, βLeu96δ1, and βLeu96δ2, respectively, surprisingly larger than the averages (0.55 and 0.52 for the α-chain and β-chain, respectively). Interestingly, both αLeu91 and βLeu96 methyl groups are proximal to hemes (Figure 3), and we observed several intermolecular NOEs between each of these methyl groups and the heme. The high S_{axis}^2 values of these methyl groups can thus be attributed to their interactions with the heme.

If the alanines are excluded, the methyl-containing residues located in the α1β1 interface include αLeu34, αVal107, αThr118, βVal33, βVal34, βMet55, βVal111, and βThr123. With the exception of αLeu34, all other residues had S_{axis}^2 values significantly higher than the averages. Only one Met residue exists in the β-chain, and its S_{axis}^2 value (0.62) is larger than the average S_{axis}^2 value of Leu methyl groups, although the

dx.doi.org/10.1021/bi4005683 | Biochemistry 2013, 52, 5809−5820

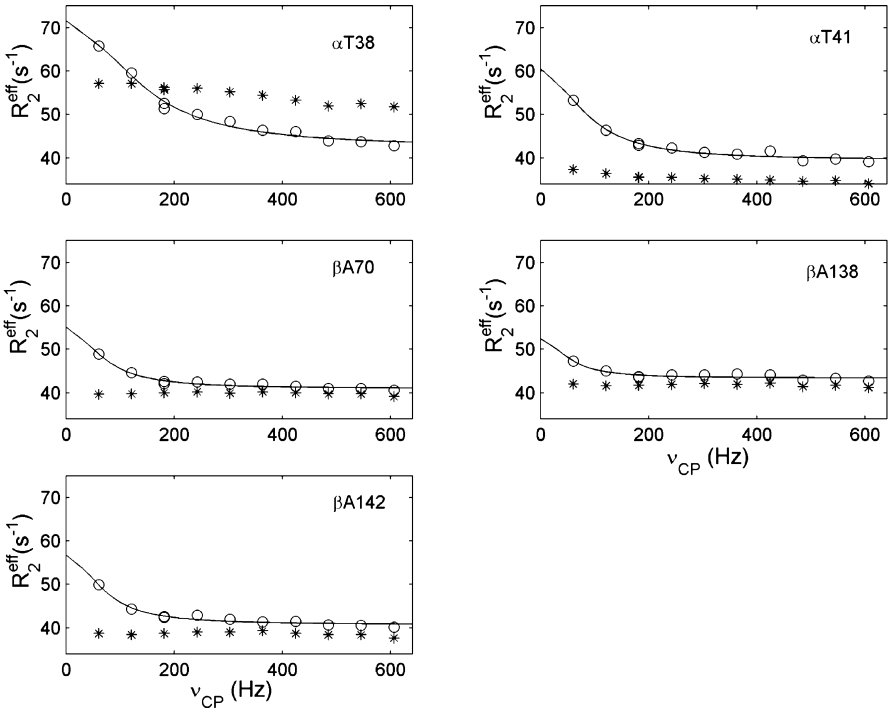

Figure 6. Relaxation dispersion profiles of the methyl groups with intrinsic conformational exchange in the absence and presence of IHP. The data collected in the samples with and without IHP are presented as circles and asterisks, respectively. The solid lines are fitting curves assuming the two-state exchange model. The identity of each residue is indicated inside each panel.

Met methyl is one bond farther from the backbone than the Leu methyl. The results indicate that the $\alpha1\beta1$ interface of HbCO A is rigid on this time scale, consistent with the backbone dynamics results and the X-ray structures. αLeu34 is located at the end of helix B, and one of its methyl groups is largely exposed to solvent, explaining its low S_{axis}^2 values (~0.34). Only three methyl-containing residues, αThr38, αThr41, and αVal96, are located in the $\alpha1\beta2$ interface. Both αThr38 and αThr41 have flexible methyl side chains as shown above. Moreover, the S_{axis}^2 values of the two methyl groups in αVal96 are 0.48 and 0.47, respectively, also significantly lower than the average (0.71). Taken together, the results demonstrate that the $\alpha1\beta2$ interface is flexible while the $\alpha1\beta1$ interface is quite rigid on picosecond to nanosecond time scales in solution. Solvent hydrogen exchange experiments,[35] though, showed that the $\alpha1\beta1$ interface is dynamic as well, albeit on a much slower time scale of milliseconds to seconds, faster in deoxy-Hb and slower in the ligated forms of Hb A. This dynamic behavior is revealed by the solvent exchange rates of the histidyl side chain NεH group of αHis103 and αHis122, and these rates increase in the presence of allosteric effectors such as IHP and inorganic phosphates or chloride ions.

Methyl Dynamics on the Millisecond to Microsecond Time Scale. Except for αThr38 and αThr41, the methyl groups of Ala, Met, and other Thr residues in HbCO A do not display relaxation dispersion in the absence of IHP. For αThr38 and αThr41, small relaxation dispersions can be observed (Figure 6), indicating that the switch region in the $\alpha1\beta2$ interface of HbCO A is dynamic on the millisecond to microsecond time scale, which is also dynamic on the nanosecond to picosecond time scales as shown above. The αThr38 methyl had a much larger effective relaxation rate than other methyl groups, but its relaxation dispersion is small over the range of CPMG field strengths from 60 to 600 Hz. This result indicates that the conformational exchange for the αThr38 methyl occurs on a time scale significantly faster than milliseconds. The conformational exchange observed here is consistent with the result obtained from a recent backbone relaxation study: αLys40 of HbCO A (in the $\alpha1\beta2$ interface) is mobile on the millisecond to microsecond time scale.[13] The mobility of this switch region was detected only for HbCO A, not for the deoxy form.[13] In the deoxy form, the positively charged side chain of αLys40 forms strong interactions with the negatively charged C-terminus of the β-chain (βHis146) according to the crystal structure, greatly reducing the mobility of the switch region. However, in the liganded form, these two residues are too distant to interact with each other in our NMR structure. As a consequence, the interactions in the $\alpha1\beta2$ interface become weaker and the interface becomes more dynamic upon Hb ligation. This conformational exchange in the $\alpha1\beta2$ interface should result from local dynamics instead of reorientation of the $\alpha1\beta1$ dimer relative to the $\alpha2\beta2$ dimer. Otherwise, more residues would display relaxation dispersion. Localized conformational exchange in the $\alpha1\beta2$ interface was also detected early for the indole NH group of βTrp37 in HbCO A in the presence of IHP.[36]

Effects of IHP Binding on Methyl Dynamics. As shown in Table 3, Figure 5, and Figure S5 of the Supporting Information, upon IHP binding, some methyl groups of HbCO A became more flexible while others became more rigid, but the average order parameters, $\langle S_{axis}^2 \rangle$, showed nearly no change [$\langle S_{axis}^2 \rangle$(free) − $\langle S_{axis}^2 \rangle$(IHP) = −0.004]. The changes in S_{axis}^2 values [S_{axis}^2(free) − S_{axis}^2(IHP)] were within a quite small range, and the maximal change was ~0.19 (Figure S5b,d of the Supporting Information). The residues with significant changes in S_{axis}^2 [$|S_{axis}^2$(free) − S_{axis}^2(IHP)| > 0.05] are distributed mainly in four regions: (i) proximal to the IHP binding sites in the α-cleft (αVal1) and β-cleft (βVal1, βLeu3, and βLeu81),

dx.doi.org/10.1021/bi4005683 | Biochemistry 2013, 52, 5809−5820

(ii) proximal to the hemes in the α-chain (αMet32, αAla65, αLeu86, and αLeu105) and β-chain (βLeu31, βVal98, βLeu106, and βLeu141), (iii) in the α1β2 interface (αThr38), and (iv) in the α1β1 interface (αLeu34, αVal107, αThr118, βVal34, and βAla115). Several residues in the αG helix (αLeu101, αLeu106, αThr108, and αLeu109), βG helix (βLeu114), and βH helix (βVal134) also displayed significant changes in S_{axis}^2 values upon the interaction of IHP with HbCO A. Although αVal1 and βVal1 are close to the IHP binding sites in the α- and β-clefts, their methyl groups may not interact directly with IHP, and the increase in their methyl mobility may arise from a structural change around the binding sites. Consistent with IHP-induced structural changes (or chemical shift changes), many methyl-containing residues in the proximity of the hemes also displayed changes in dynamics on the picosecond to nanosecond time scales. These changes should be caused by the allosteric effect instead of direct interactions with IHP. Similarly, the changes in the dynamics for the residues located in α1β1 and α1β2 interfaces and helices G and H should originate from the allosteric effect, too.

A recent MD simulation study showed that Hb became more flexible or had higher entropy upon deoxygenation and/or binding of 2,3-BPG. The estimated time scale and maximal amplitude of the fluctuation of helices E and F were of the order of ∼2 ns and ∼3 Å, respectively.[11] On the basis of this simulation, it was proposed that the concerted fluctuations of the EF helical region could modulate the position of the distal and proximal His residues relative to the heme Fe and, in turn, could modulate the oxygen affinity of Hb.[8] It was also suggested that the heterotropic allosteric effects of Hb were caused by conformational entropy changes and had little to do with quaternary structural changes.[8] According to our experimental results, IHP binding induces limited changes in the dynamics of some residues on the picosecond to nanosecond time scales. However, there were no obvious overall changes in mobility on the nanosecond to picosecond time scales for the entire protein or E/F helices upon IHP binding (Figure 5 and Figure S5 of the Supporting Information). Using the order parameters for the methyl groups in the IHP-free and -bound forms, we estimated the conformational entropy change [S(IHP) − S(free)] to be approximately −70 J mol^{-1} K^{-1} for HbCO A using the simple diffusion-in-a-cone model.[37] It is noteworthy that the entropy was calculated by considering conformational changes of only methyl groups on nanosecond to picosecond time scales and neglecting the contributions from other time scales and other groups in methyl-containing residues and other residues. A more reliable empirical calibration method has recently been proposed to estimate the conformational entropy change upon ligand binding from only methyl order parameters.[38] Using a scaling factor of 0.037 kJ mol^{-1} K^{-1} residue^{-1} established previously,[38] the conformational entroy change was found to be −85 J mol^{-1} K^{-1} for the Hb tetramer, consistent with result derived from the simple model. Becaue the scaling factor is uncertain and may be different for different proteins,[39] the entropy obtained here is just an estimation. Nevertheless, our result indicates that the conformational entropy of HbCO A should decrease or remain nearly unchanged rather than increase significantly upon IHP binding as proposed previously.[8,11] Therefore, the heterotropic allosteric effects should result mainly from both tertiary and quaternary structural changes and might be influenced slightly by changes in the dynamics on the nanosecond to picosecond time scales.

When IHP binds to HbCO A, six residues among all the Ala, Met, and Thr residues show obvious relaxation dispersion (Figure 6). One of them could not be assigned unambiguously because the methyl correlation peak of this residue is in an overlapped region in the ^{13}C−^{1}H HSQC spectrum of the α-chain in the absence of IHP. The other five residues (αThr38, αThr41, βAla70, βAla138, and βAla142) are distributed in three regions. αThr38 and αThr41 are located in the α1β2 interface. βAla70 is in close contact with the heme (Figure 3). βAla138 and βAla142 are near the heme. βAla142 is adjacent to a residue (βHis143) directly involved in IHP binding (Figure 4a). According to previous measurements of R_{ex} values for backbone amides,[13] IHP-induced conformational exchange could also be observed in these three regions: the α1β2 interface, heme binding sites, and IHP binding sites. The results indicate that HbCO A exists in two or more conformations in the presence of IHP, at least for these three regions. Early ^{31}P NMR studies[40] suggested that IHP binds sequentially to hemoglobin at multiple sites in fast exchange between them with exchange rates of >10^4 s^{-1}. The conformational exchange observed here should not correspond to those among the fully IHP-bound, partially IHP-bound, and IHP-free forms because many methyl groups displayed significant chemical shift perturbations by IHP but did not show relaxation dispersion upon IHP binding. Instead, more than one protein conformations that undergo exchange in the presence of IHP should exist. Assuming a two-state exchange model,[41] we estimated the exchange rate to be in the range of 400−800 s^{-1} (i.e., on the millisecond time scale), significantly smaller than that estimated from k_{on} and k_D for the binding of IHP to HbCO A.[40] Most likely, the conformational exchange observed here arises from the relative motion of the α1β1 dimer with respect to the α2β2 dimer. The relative motion alters the local structures (chemical shifts) around the α1β2 interface and also the heme binding sites, modulating the oxygen affinity of Hb.

■ CONCLUDING REMARKS

The structural and dynamic results presented in this paper show that (i) the classical two-structure allosteric models for hemoglobin cannot describe the mechanisms as well as the structural and dyamic aspects of the cooperative oxygen binding to Hb A and (ii) hemoglobin is a flexible molecule. This flexibility is essential for the physiological function of Hb A as an oxygen carrier. In solution, the structure of HbCO A is a dynamic ensemble of various structures. A recent wide-angle X-ray solution scattering (WAXS) investigation shows that the observed WAXS pattern for HbCO A in solution is different from those calculated from the atomic coordinate sets, suggesting the structure of this protein in solution is different from the known crystal structures,[42] consistent with our NMR structural and dynamic results.

The binding of the heterotropic allosteric effector, IHP, affects both tertiary and quaternary (intersubunit interface) structures of hemoglobin as well as the relative motion of the α1β1 dimer with respect to the α2β2 dimer but does not increase the conformational entropy. This result is significant, as the role of protein dynamics in the allosteric effect has gained an increased level of recognition recently.[43−45] It appears thus that an intricate web of multiple and highly specific interactions involving both types of intersubunit interfaces is responsible for regulating hemoglobin function. An important implication of our results is that allosteric interactions in other regulatory

proteins and enzymes will likely require multiple pathways for signal communication, with the dynamics playing a crucial role.

■ ASSOCIATED CONTENT

Supporting Information

One figure showing the stereospecific assignment of methyl groups, one figure showing the IHP binding sites and chemical shift perturbations mapped onto the ribbon structure, one figure showing peak shifts with an increase in IHP concentration, one figure showing amide hydrogen−water exchange profiles, one figure showing $S_{axis}^2 - \langle S_{axis}^2 \rangle$ in the absence of IHP and S_{axis}^2(free) − S_{axis}^2(IHP), and one table listing the RDC Q factors for 20 lowest-energy structures. This material is available free of charge via the Internet at http://pubs.acs.org.

Accession Codes

Coordinates for the refined structure of HbCO A have been deposited in the Protein Data Bank as entry 2m6z.

■ AUTHOR INFORMATION

Corresponding Author

*D.Y.: telephone, 65-65161014; e-mail, dbsydw@nus.edu.sg. C.H.: telephone, (412) 268-3395; e-mail, chienho@andrew.cmu.edu.

Funding

This work was supported by a research grant from the National Institutes of Health (R01GM084614 to C.H.) and a grant from Singapore Ministry of Education (Academic Research Fund Tier 2, R154000453112 to D.Y.).

Notes

The authors declare no competing financial interest.

■ ACKNOWLEDGMENTS

We thank Dr. Ad Bax for helpful and stimulating discussions.

■ ABBREVIATIONS

RDC, residual dipolar coupling; NOESY, nuclear Overhauser effect spectroscopy; IHP, inositol hexaphosphate; HbCO A, human adult carbonmonoxy Hb; 2,3-BPG, 2,3-bisphosphoglycerate; HSQC, heteronuclear single-quantum coherence; HMQC, heteronuclear multiple-quantum coherence; CSA, chemical shift anisotropy; CPMG, Carr−Purcell−Meiboom−Gill sequence; rmsd, root-mean-square deviation.

■ REFERENCES

(1) Monod, J., Wyman, J., and Changeux, J. P. (1965) On the nature of allosteric transitions: A plausible model. *J. Mol. Biol. 12*, 88−118.

(2) Perutz, M. F. (1970) Stereochemistry of cooperative effects in haemoglobin. *Nature 228*, 726−739.

(3) Silva, M. M., Rogers, P. H., and Arnone, A. (1992) A third quaternary structure of human hemoglobin A at 1.7-Å resolution. *J. Biol. Chem. 267*, 17248−17256.

(4) Safo, M. K., and Abraham, D. J. (2005) The enigma of the liganded hemoglobin end state: A novel quaternary structure of human carbonmonoxy hemoglobin. *Biochemistry 44*, 8347−8359.

(5) Lukin, J. A., Kontaxis, G., Simplaceanu, V., Yuan, Y., Bax, A., and Ho, C. (2003) Quaternary structure of hemoglobin in solution. *Proc. Natl. Acad. Sci. U.S.A. 100*, 517−520.

(6) Gong, Q., Simplaceanu, V., Lukin, J. A., Giovannelli, J. L., Ho, N. T., and Ho, C. (2006) Quaternary structure of carbonmonoxyhemoglobins in solution: Structural changes induced by the allosteric effector inositol hexaphosphate. *Biochemistry 45*, 5140−5148.

(7) Xu, Y., Zheng, Y., Fan, J.-S., and Yang, D. (2006) A new strategy for structure determination of large proteins in solution without deuteration. *Nat. Methods 3*, 931−937.

(8) Yonetani, T., and Laberge, M. (2008) Protein dynamics explain the allosteric behaviors of hemoglobin. *Biochim. Biophys. Acta 1784*, 1146−1158.

(9) Yonetani, T., Park, S. I., Tsuneshige, A., Imai, K., and Kanaori, K. (2002) Global allostery model of hemoglobin. Modulation of O_2 affinity, cooperativity, and Bohr effect by heterotropic allosteric effectors. *J. Biol. Chem. 277*, 34508−34520.

(10) Yokoyama, T., Neya, S., Tsuneshige, A., Yonetani, T., Park, S. Y., and Tame, J. R. (2006) R-state haemoglobin with low oxygen affinity: Crystal structures of deoxy human and carbonmonoxy horse haemoglobin bound to the effector molecule L35. *J. Mol. Biol. 356*, 790−801.

(11) Laberge, M., and Yonetani, T. (2008) Molecular Dynamics Simulations of Hemoglobin A in Different States and Bound to DPG: Effector-Linked Perturbation of Tertiary Conformations and HbA Concerted Dynamics. *Biophys. J. 94*, 2737−2751.

(12) Song, X. J., Yuan, Y., Simplaceanu, V., Sahu, S. C., Ho, N. T., and Ho, C. (2007) A comparative NMR study of the polypeptide backbone dynamics of hemoglobin in the deoxy and carbonmonoxy forms. *Biochemistry 46*, 6795−6803.

(13) Song, X. J., Simplaceanu, V., Ho, N. T., and Ho, C. (2008) Effector-induced structural fluctuation regulates the ligand affinity of an allosteric protein: Binding of inositol hexaphosphate has distinct dynamic consequences for the T and R states of hemoglobin. *Biochemistry 47*, 4907−4915.

(14) Simplaceanu, V., Lukin, J. A., Fang, T. Y., Zou, M., Ho, N. T., and Ho, C. (2000) Chain-selective isotopic labeling for NMR studies of large multimeric proteins: Application to hemoglobin. *Biophys. J. 79*, 1146−1154.

(15) Neri, D., Szyperski, T., Otting, G., Senn, H., and Wuthrich, K. (1989) Stereospecific nuclear magnetic resonance assignments of the methyl groups of valine and leucine in the DNA-binding domain of the 434 repressor by biosynthetically directed fractional ^{13}C labeling. *Biochemistry 28*, 7510−7516.

(16) Hwang, T. L., van Zijl, P. C., and Mori, S. (1998) Accurate quantitation of water-amide proton exchange rates using the phase-modulated CLEAN chemical EXchange (CLEANEX-PM) approach with a Fast-HSQC (FHSQC) detection scheme. *J. Biomol. NMR 11*, 221−226.

(17) Zhang, X., Sui, X., and Yang, D. (2006) Probing methyl dynamics from ^{13}C autocorrelated and cross-correlated relaxation. *J. Am. Chem. Soc. 128*, 5073−5081.

(18) Yang, D. (2011) Probing protein side chain dynamics via ^{13}C NMR relaxation. *Protein Pept. Lett. 18*, 380−395.

(19) Lundström, P., Vallurupalli, P., Religa, T. L., Dahlquist, F. W., and Kay, L. E. (2007) A single-quantum methyl ^{13}C-relaxation dispersion experiment with improved sensitivity. *J. Biomol. NMR 38*, 79−88.

(20) Delaglio, F., Grzesiek, S., Vuister, G. W., Zhu, G., Pfeifer, J., and Bax, A. (1995) NMRPipe: A multidimensional spectral processing system based on UNIX pipes. *J. Biomol. NMR 6*, 277−293.

(21) Schwieters, C. D., Kuszewski, J. J., Tjandra, N., and Clore, G. M. (2003) The Xplor-NIH NMR molecular structure determination package. *J. Magn. Reson. 160*, 66−74.

(22) Zweckstetter, M., and Bax, A. (2000) Prediction of sterically induced alignment in a dilute liquid crystalline phase: Aid to protein structure determination by NMR. *J. Am. Chem. Soc. 122*, 3791−3792.

(23) Trott, O., and Olson, A. J. (2010) AutoDock Vina: Improving the speed and accuracy of docking with a new scoring function, efficient optimization and multithreading. *J. Comput. Chem. 31*, 455−461.

(24) Morris, G. M., Huey, R., Lindstrom, W., Sanner, M. F., Belew, R. K., Goodsell, D. S., and Olson, A. J. (2009) Autodock4 and AutoDockTools4: Automated docking with selective receptor flexibility. *J. Comput. Chem. 16*, 2785−2791.

(25) Mueser, T. C., Rogers, P. H., and Arnone, A. (2000) Interface sliding as illustrated by the multiple quaternary structures of liganded hemoglobin. *Biochemistry 39*, 15353−15364.
(26) Srinivasan, R., and Rose, G. D. (1994) The T-to-R transition in hemoglobin: A reevaluation. *Proc. Natl. Acad. Sci. U.S.A. 91*, 11113−11117.
(27) Fan, J. S., Cheng, Z., Zhang, J., Noble, C., Zhou, Z., Song, H., and Yang, D. (2009) Solution and crystal structures of mRNA exporter Dbp5p and its interaction with nucleotides. *J. Mol. Biol. 388*, 1−10.
(28) Zuiderweg, E. R. P., Hamers, L. F., Bruin, S. H. d., and Hilbers, C. W. (1981) Equilibrium aspects of the binding of myo-inositol hexakisphosphate to human hemoglobin as studied by ^{31}P NMR and pH-Stat techniques. *Eur. J. Biochem. 118*, 85−94.
(29) Arnone, A., and Perutz, M. F. (1974) Structure of inositol hexaphosphate-human deoxyhaemoglobin complex. *Nature 249*, 34−36.
(30) Laberge, M., Kovesi, I., Yonetani, T., and Fidy, J. (2005) R-state hemoglobin bound to heterotropic effectors: Models of the DPG, IHP and RSR13 binding sites. *FEBS Lett. 579*, 627−632.
(31) Nagatomo, S., Nagai, M., Mizutani, Y., Yonetani, T., and Kitagawa, T. (2005) Quaternary structures of intermediately ligated human hemoglobin A and influences from strong allosteric effectors: Resonance Raman investigation. *Biophys. J. 89*, 1203−1213.
(32) Kay, L. E., Torchia, D. A., and Bax, A. (1989) Backbone dynamics of proteins as studied by ^{15}N inverse detected heteronuclear NMR spectroscopy: Application to staphylococcal nuclease. *Biochemistry 28*, 8972−8979.
(33) Yang, D., Mittermaier, A., Mok, Y. K., and Kay, L. E. (1998) A study of protein side-chain dynamics from new ^{2}H auto-correlation and ^{13}C cross-correlation NMR experiments: Application to the N-terminal SH3 domain from drk. *J. Mol. Biol. 276*, 939−954.
(34) Kay, L. E., Muhandiram, D. R., Farrow, N. A., Aubin, Y., and Forman-Kay, J. D. (1996) Correlation between dynamics and high affinity binding in an SH2 domain interaction. *Biochemistry 35*, 361−368.
(35) Mihailescu, M.-R., and Russu, I. M. (2001) A signature of the T → R transition in human haemoglobin. *Proc. Natl. Acad. Sci. U.S.A. 98*, 3773−3777.
(36) Yuan, Y., Simplaceanu, V., Lukin, J. A., and Ho, C. (2002) NMR investigation of the dynamics of tryptophan side-chains in hemoglobins. *J. Mol. Biol. 321*, 863−878.
(37) Yang, D., and Kay, L. E. (1996) Contributions to conformational entropy arising from bond vector fluctuations measured from NMR-derived order parameters: Application to protein folding. *J. Mol. Biol. 263*, 369−382.
(38) Marlow, M. S., Dogan, J., Frederick, K. K., Valentine, K. G., and Wand, A. J. (2010) The role of conformational entropy in molecular recognition by calmodulin. *Nat. Chem. Biol. 6*, 352−358.
(39) Tzeng, S. R., and Kalodimos, C. G. (2012) Protein activity regulation by conformational entropy. *Nature 488*, 236−240.
(40) Zuiderweg, E. R. P., Hamers, L. F., Rollema, H. S., Bruin, S. H. D., and Hilbers, C. W. (1981) ^{31}P NMR study of the kinetics of binding of myo-inositol hexakisphosphate to human hemoglobin: Observation of fast-exchange kinetics in high-affinity systems. *Eur. J. Biochem. 118*, 95−104.
(41) Carver, J. P., and Richards, R. E. (1972) A general two-site solution for the chemical exchange produced dependence of T_2 upon the Carr−Purcell pulse separation. *J. Magn. Reson. 6*, 89−105.
(42) Makowski, L., Bardhan, J., Gore, D., Lal, J., Mandava, S., Park, S., Rodi, D. J., Ho, N. T., Ho, C., and Fischetti, R. F. (2011) WAXS studies of the structural diversity of hemoglobin in solution. *J. Mol. Biol. 408*, 909−921.
(43) Kern, D., and Zuiderweg, E. R. P. (2003) The role of dynamics in allosteric regulation. *Curr. Opin. Struct. Biol. 13*, 748−757.
(44) Boehr, D. D., Nussinov, R., and Wright, P. E. (2009) The role of dynamic conformational ensembles in biomolecular recognition. *Nat. Chem. Biol. 5*, 789−796.
(45) Tzeng, S.-R., and Kalodimos, C. G. (2011) Protein dynamics and allostery: An NMR view. *Curr. Opin. Struct. Biol. 21*, 62−67.
(46) Koradi, R., Billeter, M., and Wuthrich, K. (1996) MOLMOL: A program for display and analysis of macromolecular structures. *J. Mol. Graphics 14*, 29−32.
(47) Laskowski, R. A., Rullmannn, J. A., MacArthur, M. W., Kaptein, R., and Thornton, J. M. (1996) AQUA and PROCHECK-NMR: Programs for checking the quality of protein structures solved by NMR. *J. Biomol. NMR 8*, 477−486.